Supporting Information

for

Path-dependent morphology of CH_4 hydrates and their dissociation studied with high-pressure microfluidics

Jidong Zhang[1], Zhenyuan Yin[1,], Saif A. Khan[2], Shuxia Li[3], Qingping Li[4],*

Xiaohui Liu[1], Praveen Linga[2]

[1] Institute for Ocean Engineering, Shenzhen International Graduate School, Tsinghua University, Shenzhen 518055, China

[2] Department of Chemical and Biomolecular Engineering, National University of Singapore, Singapore 117582, Singapore

[3] School of Petroleum Engineering, China University of Petroleum (East China), Qingdao 266580, China

[4] State Key Laboratory of Natural Gas Hydrates, Technology Research Department CNOOC Research, Beijing 100192, China

*Corresponding author: Z. Yin (zyyin@sz.tsinghua.edu.cn).

No. of Pages: 11

No. of Sections: 4

No. of Figures: 8

Section 1. Experimental apparatus and material

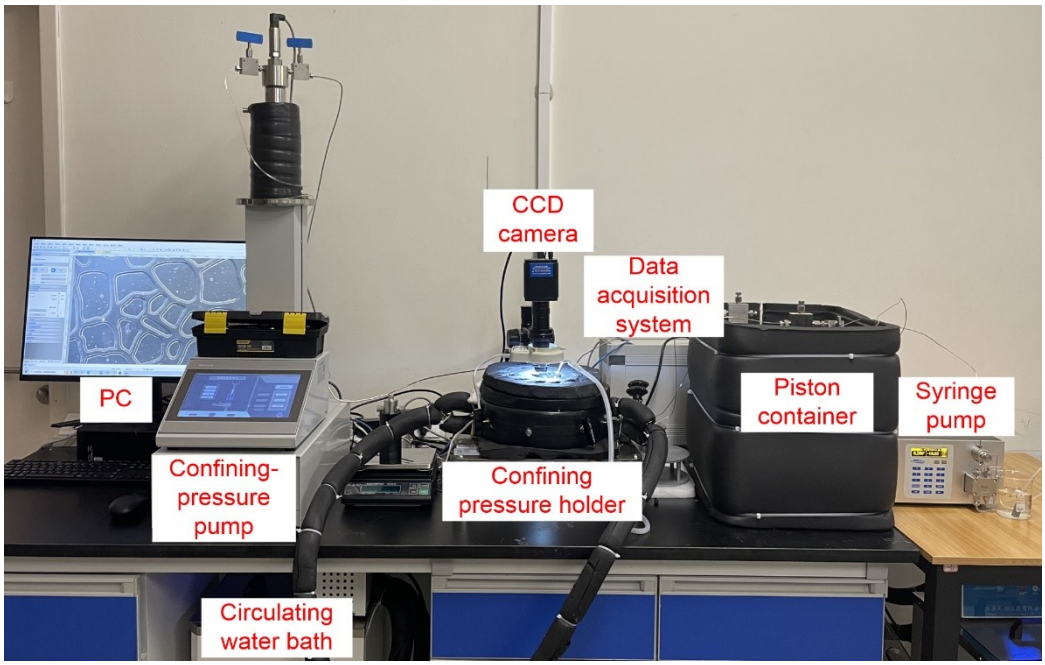

Fig. S1. Picture of the in-house made high-pressure microfluidics experimental apparatus.

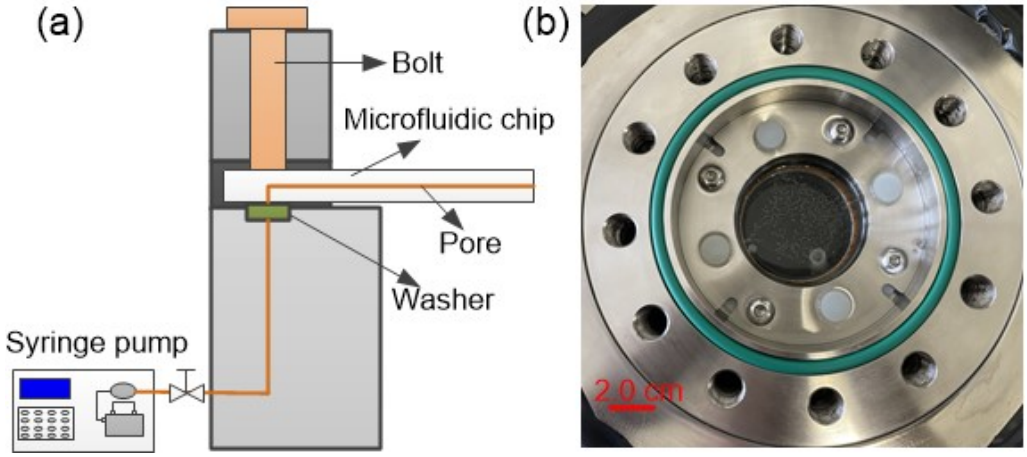

Fig. S2. (a) Schematic of the interface of the microfluidic chip and constant flow-rate syringe pump. (b) A picture of the confining pressure holder used in this study.

Fig. S3a presents the geometry model of the microfluidic chip device, including the insulation layer, reactor wall, circulating water bath, and micro-fluidic chip. Blowing tubes are positioned at the upper and lower ends of the reactor to effectively disperse the condensation on the glass surface. In this study, COMSOL Multiphysics, a finite element-based solver, was utilized to conduct the CFD simulations using a steady-state approach. Fig. S3b shows the isotherm of the 3-D geometry model. The temperature inside the reactor is non-uniformly distributed due to the influence of the environment and the continuous blowing of the glass surface. Consequently, the temperature of the field view area is not consistent with the temperature of the thermocouple measurement point. Therefore, we simulated the temperature distribution inside the reactor at different circulating water bath temperatures by CFD simulation.

In addition, we have performed a statistical analysis of the accuracy between the simulation results and experimental results. The absolute mean difference deviation (*AARD*) was calculated by the following equation:

$$AARD = \frac{1}{n}\sum_{i=1}^{n}\frac{\left|T_i^{sim} - T_i^{exp}\right|}{T_i^{exp}}$$

Where n represents the number of simulation data points, T_i^{sim} and T_i^{exp} are the simulation results and experimental results, respectively. Fig. S3c compares the temperature among experimental and simulation at thermocouples. It demonstrates unequivocally that the simulation results are consistent with the experimental results, which indicates that the simulation is in good agreement with a minimum $AARD = 0.3\%$ compared with the simulation results. Fig. S3d depicts the correlation between the temperature measured by the thermocouple and the temperature at the field of view location. As can be seen, there exists a linear relationship between the temperature recorded by the thermocouple and the corresponding temperature at the field of view. We utilized this equation to calibrate the experimental data during both methane hydrate formation and dissociation processes.

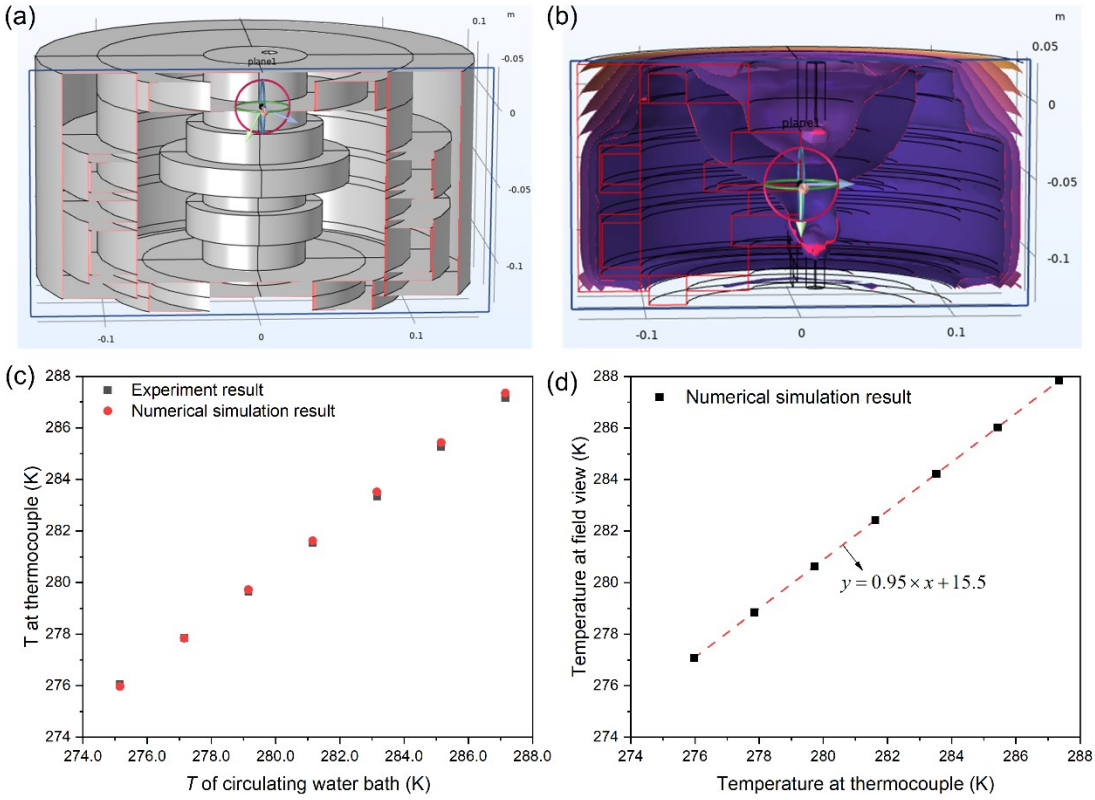

Fig. S3. (a) Schematic of a reconstructed 3-D geometric model of microfluidic experimental apparatus; (b) isotherm of 3-D microfluidic chip device based on CFD stimulation; (c) comparison of experiment and simulation temperature between circulating water bath and thermocouple; (d) the relation of temperature between field view and thermocouple based on CFD simulation.

The size of the microfluidic chip is 76.0 × 76.0 × 4.0 mm with inlet and outlet ports at two diagonals. The etched area occupies 40.0 × 40.0 mm with a depth of 100.0 μm. The fabrication of the microfluidic chip used a combined technology of both laser etching followed by wet etching as the etched flow channel has a large variation in pore width (minimum width of 100 μm and maximum width of 500 μm) compared with a constant pore depth of 100 μm. The key steps for a microfluidic chip fabrication are as follows with a schematic shown in Fig. S4 in Supporting Information:

a. Deposit a metal film onto a clean glass substrate following a cleaning process consisting of a 10-min ultrasonic cleaning in acetone and isopropyl alcohol and a 5-min plasma treatment;

b. Based on the detailed flow channel specification, UV laser was tuned to etch the surface of the metal film layer;

c. Etch the laser-patterned channels with rough surface using hydrofluoric acid solution for 2 hours, followed by cleaning the coating metal film;

d. Use a dicing saw to separate the glass chip into the designed microfluidic chip size. Clean both the top and bottom glass surfaces using a 10-min ultrasonic method in acetone and isopropyl alcohol followed by a 5-min plasma treatment;

e. Bond the two glass chips using a direct wafer bonding machine at a high vacuum (72.0 kPa) while heating to 573.0 K and retrieve the microfluidic chip from the vacuum chamber.

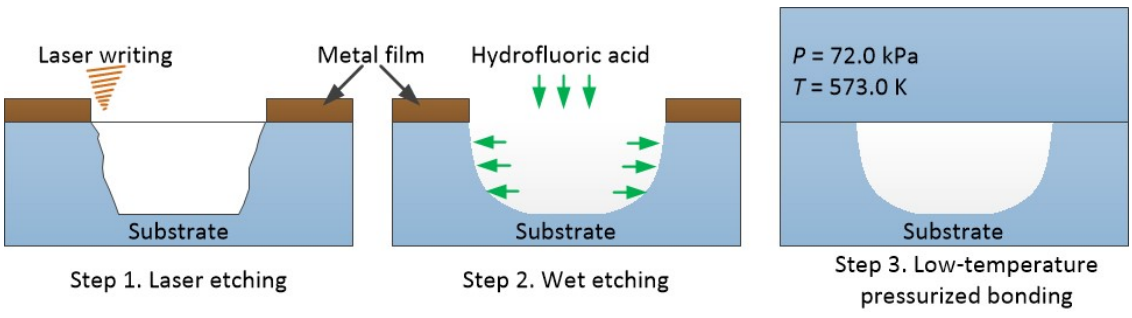

Fig. S4. Schematic of the key steps involved in fabrication of a microfluidic chip used in this study.

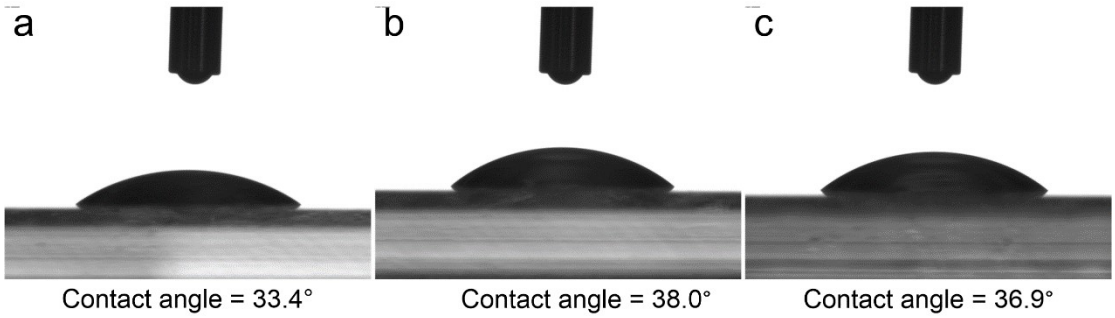

Fig. S5. Contact angle of micro-fluidic chip used in this study with average $\theta = 36.1°$, (a) $\theta = 33.4°$, (b) $\theta = 38.0°$, (c) $\theta = 36.9°$.

Section 2. Experimental procedure

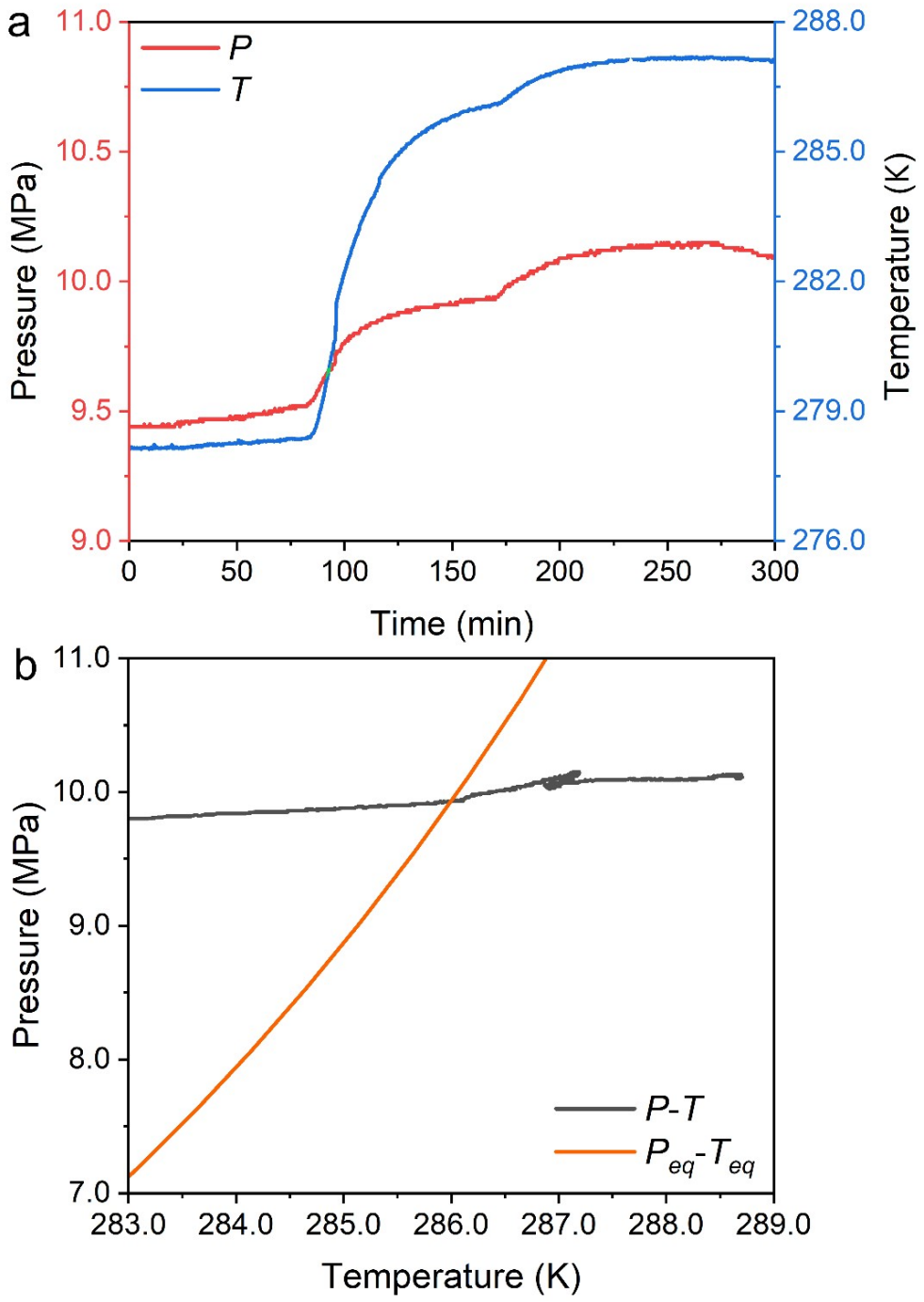

Fig. S6. (a) Evolution of *P* and *T* over time; (b) *P*-*T* trace in relation to CH_4 hydrate equilibrium curve in the process of MH dissociation induced by thermal stimulation.

Section 3. MH formation from CH_4 gas bubble

Fig. S7 shows the gas-liquid-hydrate interface before the MH film rupture. We obtained the gas bubble and hydrate film dimensions based on ImageJ software. However, due to the uncertainty of size in the z-direction, we assume that the depth of the gas bubble and MH film is consistent with the depth of the pore channel (H = 100 μm).

According to the above assumptions, the equation for calculating the volume of the gas bubble and MH film can be expressed as follows:

$$V_G = L_G \times W_G \times H = 3.4 \times 10^{-5} \text{ mL}$$

$$V_H = 2 \times (L_G + W_G) \times W_H = 6.0 \times 10^{-6} \text{ mL}$$

The pore-volume balance method developed by Yin et al.[1] was used to estimate the pressure change in a gas bubble. In this method, the molar moles of CH_4 were estimated using the Peng-Robinson (PR) equation of state. Based on the assumption that pore volume remained constant throughout the process, MATLAB R2019b was used to solve the nonlinear equation of P and T for converting CH_4 to MH. The initial pressure is 8.9 MPa, the temperature is 274.5 K. The gas bubble volume (V_G) is the initial pore volume.

Utilize MATLAB to calculate the gas consumption of a specific MH film volume (V_H) and yield ~3.2 MPa of gas bubble pressure drop caused by MH film formation.

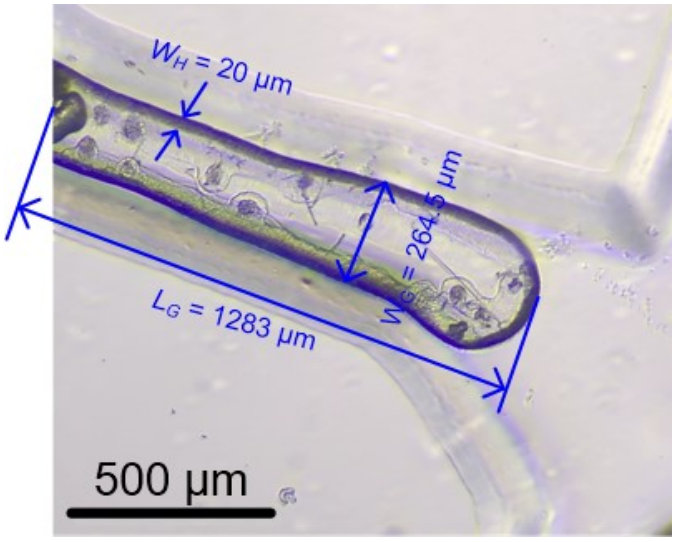

Fig. S7. The interface and dimensions of the gas-liquid-MH film.

Section 4. Analysis of micro gas bubble evolution during MH dissociation

Fig. S8 shows the method of extraction and statisticians of micro gas bubbles during MH dissociation. The image is converted to grayscale using the "rgb2gray" function in MATLAB R2019b. We employ the command "imbinarize" to create a binary image from the two-dimensional grayscale image. Based on the actual size of the image and the image pixels, we counted the bubbles in the binary image, as shown in Fig. S6c.

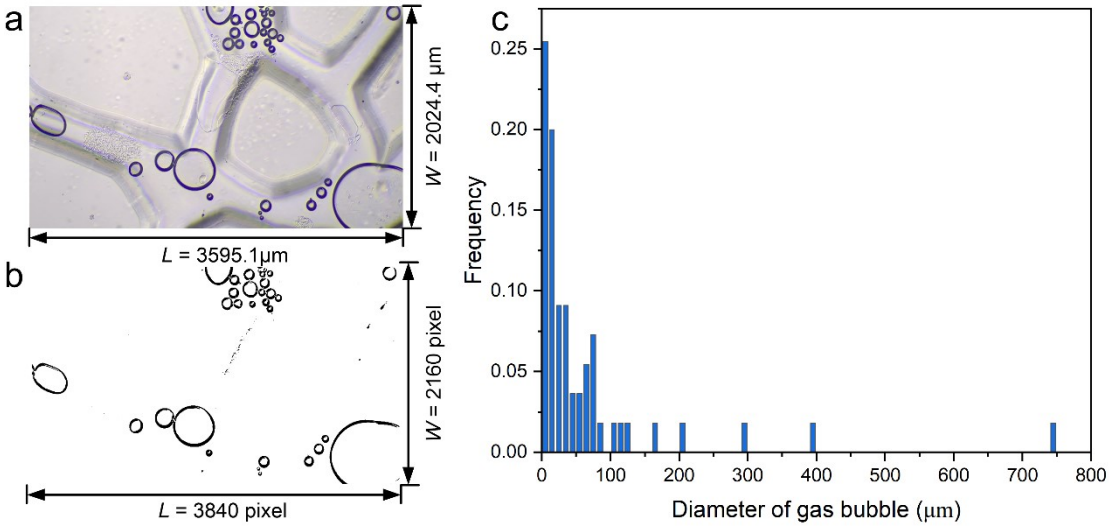

Fig. S8. The extraction method of micro gas bubble, (a) original image by CCD camera, (b) image with grayscale, (c) evolution of the frequency of micro gas bubble.

Video S1: A video showcasing the detailed morphology transition process of MH dissociation in Path I under thermal stimulation at T = 287.8 K.

Video S2: A video showing the entire MH formation process at position 1 on the microfluidic chip.

Video S3: A video showing the recrystallization process of micro-porous MH_{Bub}.

Video S4: A video showing the entire MH dissociation process in Path II under thermal stimulation at T = 287.8 K.

Video S5: A video showing the entire micro gas bubble evolution on the microfluidic chip.

References

1. Z. Yin, Q.-C. Wan, Q. Gao and P. Linga, *Applied Energy*, 2020, **271**, 115195.